Topical Review

Tailoring the electronic properties of semiconducting nanocrystal-solids

Emilio Scalise

Department of Materials Science, University of Milano-Bicocca, Via Roberto Cozzi 55, 20125 Milan, IT

E-mail: emilio.scalise@unimib.it

September 2019

Abstract. An overview of the recent progress made in the synthesis of colloidal semiconducting nanocrystals (NCs), with particular emphasis on applications for solar cell materials is provided. Peculiar phenomena in NCs, such as Multiple Exciton Generation (MEG) and Intermediate-band (IB) absorption are described as important mechanisms to improve the efficiency of the **third- generation** solar cells. The state of art and challenges to exploit these effects in NCs based materials are highlighted. We focus on two complementary approaches that are very promising: the synthesis of core/shell NCs and the incorporation of these NCs into semiconducting matrices, thus creating a fully inorganic quantum dot **solid**. We also show two examples of inorganic quantum dot solids, one using Si or Ge NCs and another employing InAs or InP NCs. For the latter, a joint experimental and theoretical study is reviewed, showing how quantum dot solids introduce new concepts and need for a new way of thinking different **than** that just summing up the effects and properties of NCs and the semiconducting hosting matrix.

Submitted to: *Semicond. Sci. Technol.*

1 Introduction: semiconducting nanocrystals for emerging photonics

Silicon and few other semiconducting bulk crystals are the most important and widely used materials in current electronic devices. Still, the increasing demand of cost-efficient electronics, sensors and systems for energy harvesting and conversion, motivates great research efforts for alternative solutions. In this context, lower dimensional materials are very appealing. Particularly, 0-2D semiconducting nanostructures exhibit uncommon physical proprieties originating from quantum confinement effect, which are often very promising for novel optoelectronic devices[1–4]. But low dimensional nanostructures typically have higher manufacturing processes costs and increase the complexity due to their puzzling integration into the devices, as compared to bulk semiconductors.
Recent advances in wet chemistry techniques [5–8] empowered a facile and economic

synthesis of colloidal semiconducting nanocrystals (NCs). These techniques introduced a new paradigm: the use of colloidal nanocrystals as 'artificial atoms' to form new NC-based solids by self-assembly. Different **aspects** of the NCs can be tuned to design **nanocrystalline** solids with tailored properties. Typically, the size of the NCs, which has **a** direct impact on the quantum confinement effect, but also their shape and the material composition can be controlled by colloidal techniques [9, 10]. By modification or exchange of the organic ligands, traditionally used for the synthesis of the NCs, also the surface and the mechanism driving the self-assembly of the NCs into **superlattices** can be tuned [11]. This is very relevant for applications, because the native organic ligands, often composed of long hydrocarbon chains, crate an insulating path between the NCs, thus degrading the conductivity of the NC composite. On the contrary, different **approaches** to improve charge-carries transport in the nanocomposites are possible such as assembling the NC into superlattices with specific structures, reducing the distance between the NCs or exchanging the long ligands with shorter or conductive inorganic ligands.

Recently, we showed that surface chemistry processes related to the organic-**inorganic** ligands exchange does lead to the formation of all-inorganic nanocrystalline solids with unique electronic and transport properties [12]. In fact, the inorganic ligands attached to the NC surface immediately dissociate during the ligand exchange process with the formation of buried interfaces, which may introduce surface states and open new charge-carrier channels. Moreover, the formation of an amorphous matrix from the dissociated ligands **creates** a heterojunction between the NCs and the hosting matrix which can be designed by tuning the wet chemistry processes to obtain properties particularly favourable for optical applications. Particularly, we showed that the heterojunction between InAs NCs and the amorphous matrix formed from Sn_2S_6 ligands is a type II heterojunction [12]. Similarly, in a recent theoretical **study,** S. Wippermann *et al.* [13] reported on the possibility to form type II heterojunctions by embedding silicon NCs into amorphous, non-stoichiometric ZnS. These heterostructures may be favourable for exciton dissociation and thus they are optimal candidates to enhance carrier multiplication processes. An alternative terminology for carrier multiplication is multiple exciton generation (MEG), and it is introduced in Section 2. In Section 3 we describe another concept that may take advantages of the interfaces formed in the NC-solids and that is very promising for **next-generation** solar cells: the intermediate band (IB) photon absorption. **Finally,** we review few systems based on colloidal nanoparticles, including the InAs/Sn_2S_6 and Si/ZnS NC-solids, which have been proposed recently **to** exploit these mechanisms for energy harvesting applications.

2 Multiple Exciton Generation

Two main loss mechanisms limit the efficiency of conventional photovoltaic devices: absorption of high energy photons creates hot excitons, but the energy exceeding the bandgap of the semiconductor is converted to vibrational energy (i.e. phonons), thereby

heating the solar cell (see figure 1a); photons with energy below the bandgap of the semiconductor are not adsorbed. To reduce **these** losses, multiple active layers can be used in the photovoltaic device, each optimized for a certain portion of the solar spectrum. These devices, **so-called** multi-junction solar cells, have a theoretical limit exceeding 66% efficiency [14]. However, the fabrication cost of multi-**junction** solar cells is an issue hindering their large-scale commercial production. On the contrary, conventional single junction solar cells have a maximum theoretical efficiency of about 33% (i.e. the Shockley Queisser limit [15]), and recently silicon solar cells have reached an efficiency over 26% [16], thus very close to the SQ limit.

Several other approach, other than multi-stacking solar cells, have been proposed to overcome the SQ limit and they can be grouped in two categories: down-conversion and up-conversion approaches. The up-conversion approaches look at the loss of below-gap photons and a promising idea is discussed in the next section. Besides, the most promising down-conversion approaches exploit the carrier multiplication effect to prevent cooling of hot carriers and thus avoid the complete loss of the above-gap photon energy [17, 18]. This approach is also named multiple exciton generation because the energy of the high-energy photons is distributed over multiple carrier pairs, thus generating multiple excitons per absorbed photon (see figure 1b). A similar mechanism in bulk semiconductors has been explained since the 1950s [19] as impact ionization, but it is a very inefficient process. In fact, in most bulk semiconductors only a negligible part of the hot excitons **succeeds** in transferring **the** exceeding kinetic energy to a second charge-carrier pair, while the other dominant part dissipates the excess of kinetic energy to lattice vibrations on ultra-fast timescale [20]. A general condition for the generation of multiple excitons is imposed by the conservation of energy in the ideal case **scenario** when an absorbed photon **generates** two excitons without any energy waste. The minimum threshold photon energy for MEG is thus $E_{th} = 2E_g$, where E_g is the energy gap of the semiconductor. However, it has been shown that in a typical solar cell (based on bulk semiconductors) the activation of MEG occurs for **energies** of the incident photon of five times the energy gap of the semiconductor [17, 21], but this corresponds to adsorption of short-wavelength light that **is** outside the solar spectrum.

2.1 Using NCs to enhance MEG

Exploiting nanocrystals is an effective way to reduce the E_{th} and enhance the MEG, thus increasing the ratio between the number of generated electrons and the number of absorbed photons (so-called quantum yield, QY) in the photovoltaic cells, and it was first proposed by Nozik [22] and then it was confirmed by different experiments [23–27]. A general and unified theory explaining MEG in nanostructures is still missing, but there is a **consensus** on the enhancement of MEG in structures where the quantum confinement effect emerges. The main reason may be attributed to the relaxation of the crystal momentum conservation rule in nanostructures, allowing for decreasing the

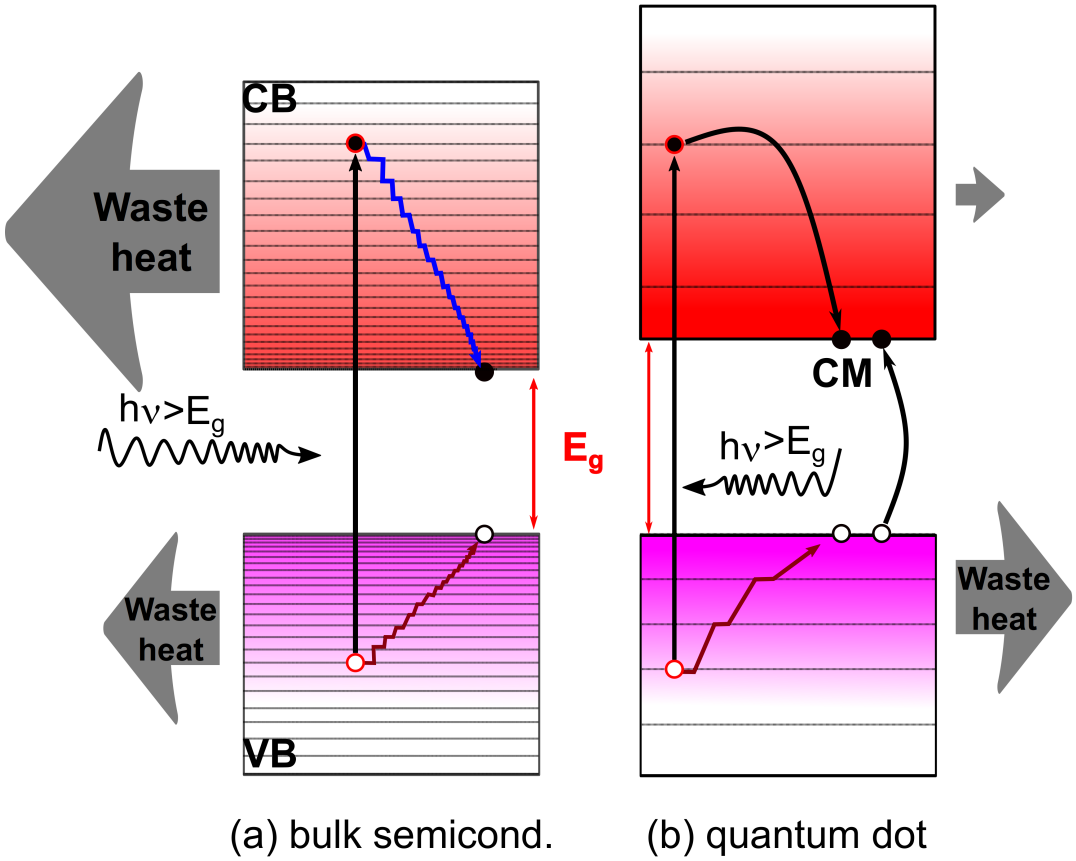

Figure 1. Schematics of photon absorption and photogenerated hot charge carriers in bulk semiconductor **a)** and quantum dot **b)**

E_{th} below the momentum conservation limit of bulk materials [21]. Other aspects that are typically considered as enhancing factors for MEG in nanocrystals are: a. enhanced Coulomb interactions in nanocrystals that favours the coupling between excitons; b. the larger spacing between the energy states in nanocrystals, which may reduce phonon-mediated relaxation (so called "phonon bottleneck" [28]).

However, these effects may be mitigated by other mechanisms that should be taken into account [29]. Particularly, enhanced Coulomb interactions provide also Auger-like relaxation channels [30], due to the typical large difference between the effective mass of electrons and holes: hot electrons can transfer their excess kinetic energy to thermalized holes, which can then cool quickly because of their higher effective mass. An approach to reduce these Auger relaxation channels consists **of** separating spatially electrons and holes, for instance by core-shell nanoparticles, which is discussed below.

Moreover, phonon bottleneck may be not very effective for MEG because of the high excess energies necessary to activate MEG: the energy levels at these high energies may be sufficiently dense (as in bulk) to allow fast relaxation via phonon emission [31]. **Nevertheless,** PbSe nanocrystals have been shown to exhibit QY above the unity (∼1.8) at about four times their bandgap [32]. This was in agreement with previous studies on lead **chalcogenide** nanocrystals showing that PbS and PbSe quantum dots

(QDs) exhibit an absorption peak at photon energies corresponding to the Σ transition (peculiar to PbSe and PbS), which was interpreted as a temporal accumulation of charge carriers due to a slowing down of charge carrier cooling. This cooling bottleneck is due to the high-energy point in the PbS and PbSe band structure at which the relaxing charge carriers would need to change the direction of the scattering wave vector **to** emit phonons [33].

3 Intermediate band solar cells

The most promising up-conversion proposal, which consists in the absorption of sub-gap photons by an intermediate band (IB), has been investigated by Luque et al. [34], who estimated an efficiency corresponding to the SQ model of about 63.1% under full concentration. The corresponding band diagram of the structure proposed is illustrated in figure 2: in between the semiconductor valence band (VB) and conduction band (CB), an additional intermediate band is present. Due to the IB, the absorption of photons is possible not only by the typical electron transition between the VB and the CB (process **labelled** as A_{VC} in figure 2), but also by transition between the Intragap state (IgS) and the CB (A_{IC} process) and between the VB and IgS (A_{VI} process). The optimal gap (E_{VC}) was determined to be about 1.93 eV, with the IB positioned at about 0.7 eV (E_{VI}). The SQ limit was estimated to be about 46.8% for one-sun with an optimal gap E_{VC}=2.4 eV and an IB energy E_{VI}=0.9 eV [35]. However, the IB absorption

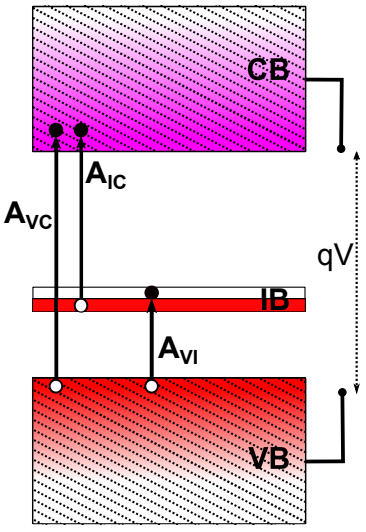

Figure 2. Band diagram of an IB solar cell, adapted with permission from [34], Copyright 1997 by the American Physical Society.

processes **is** permitted if: (1) the IgS is partially filled; (2) the transitions are optically active. Different realizations have been proposed to introduce the IgS and fulfil these two conditions, including III-V and II-VI based thin film or quantum dot arrays[35]. The latter were mostly obtained by epitaxial growth of QDs incorporated in multilayer heterostructures and their effectiveness in up-conversion was proved by different studies

[35, 36]. However, a challenge of IB solar cells obtained by epitaxial QD is the high-density of the QD arrays, which is necessary to guarantee strong absorption of the IB material. Moreover, the QD-QD distance is typically in the order of tens of nanometers in the epitaxial QD arrays, preventing the formation of the IB from the intermediate states of the isolated dots. Another non-trivial problem of epitaxial QD-based devises is the complex fabrication process, raising the cost of QD-based IB solar cells.
Recently, colloidal nanoparticles have been studied and proposed as a facile and effective implementation of the IB concept [37]. They have potentially different advantages over the epitaxial QD arrays. In fact, the possibility to form several layers of closely packed particles by few-steps of a low-temperature solution-based process allows for increasing the density of the nanoparticles, resulting in a cost reduction of the final devices. Additionally, a **fine-tuning** of the nanoparticles inter-distance at the sub-nanometer scale by ligands engineering[11, 38, 39] is also possible. The IB states could be implemented in the colloidal nanoparticles by different approaches [37]:

(i) by using polydisperse colloidal nanoparticles [40];
(ii) by introducing deep-level dopants into the nanoparticles [41];
(iii) by forming core/shell nanoparticles [24], further discussed below;
(iv) by exploiting the surface reconstructions of the nanoparticles [12, 42].

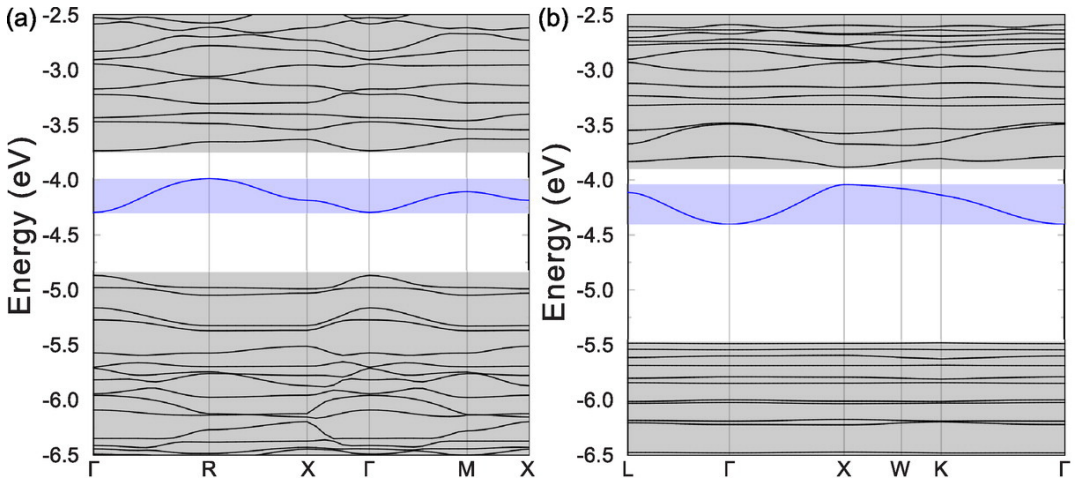

Figure 3. Band structure of a simple-cubic (SC) **a)** and a face-centered cubic (FCC) **b)** $Cd_{15}Se_{15}$ NP array along high-symmetry lines, reprinted with permission from [37]. Copyright (2015) American Chemical Society.

Introducing the IB states by exploiting the surface states of the nanoparticles is particularly interesting because this strategy does not need for ad hoc process steps to create the IB, contrary to the other three strategies. **The** nanocrystal surface has to be treated (passivated) by ligand engineering, which is a crucial step to improve the performances of solar cells based on colloidal nanoparticles [39]. Thus, designing the nanocrystal surface, by exchange, modification or removal of the ligands, with the additional aim of introducing the IB states may be not a difficult and expensive task.

As a proof of that, theoretical studies performed by Voros *et al.* [37] revealed that, due to surface reconstruction and quantum confinement, CdSe nanoparticles exhibit states well separated from the HOMO and LUMO states, which generate an IB when an array of nanoparticles is considered, as illustrated in figure 3. The theoretical predictions show that both the transitions from the IB to the CB and from the VB to the IB state are optically active. Finally, by partially filling the IB states, either by photodoping or charge doping [43, 44], surface states of colloidal nanoparticles, e.g. CdSe nanoparticles, may be considered very promising for implementing IB solar cells. We show below that exploiting the surface chemistry of the colloidal nanoparticles, which substantially modifies the surface of the nanoparticles, is a promising approach to engineering IB states in semiconducting nanocrystal-solids.

The exploitation of colloidal nanoparticles for IB solar cells does not exclude the enhancement that those nanocrystals may have on the carrier multiplication processes. Thus, a next step to fully exploit the potentialities of colloidal nanoparticles for solar cells may be the demonstration that they are optimal **platform** for up- and down-conversion at the same time. In figure 4 the band diagram of an IB solar cell is illustrated with

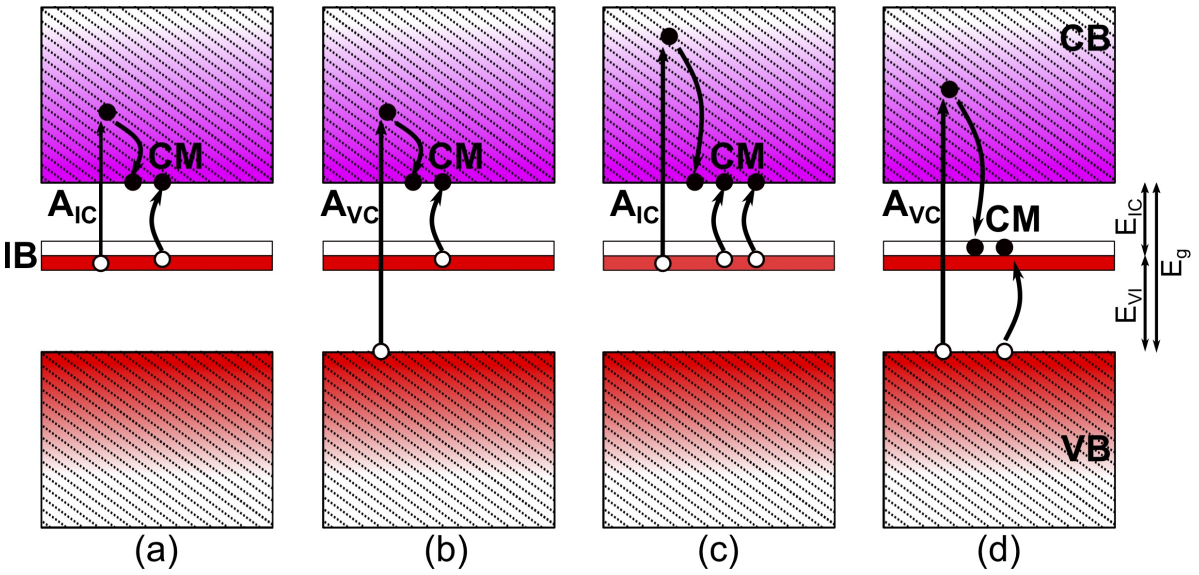

Figure 4. Band diagram of an IB solar cell and including possible carrier multiplication processes.

possible carrier **multiplication** processes that can be activated. Particularly, if the energy of absorbed photon from the IgS to the CB is larger than two times the gap between the IB and the CB minimum (E_{IC}), than MEG can be activated and two excitons are created, with the two holes generated occupying the IgS (see Figure 4**a)**. When the absorbed photon has an energy larger than ($E_g + E_{IC}$), than MEG may also be activated: the excess kinetic energy of generated hot carriers (e.g. generated hot electron in the CB as in figure 4b) can generate another electron-hole pair in between the IB and the CB. In general, if this excess energy is equal to two or more times the E_{IC}, then two or more electron-hole pair in between the IB and the CB can be generated

as shown in figure 4c. In this schema, the hot carriers are supposed to be generated in between the IB and the CB by a photon with energy larger than $3E_{IC}$. The hot carrier excess energy may also activate a transition of an electron from the VB to the IB, thus creating a second electron-hole pair (see figure 4d). In the latter case, the hot carriers (e.g. electron) must have excess energy equal to E_{VI}. By losing this excess energy, the hot electron can than still occupy the CB (if the photon energy is larger than $E_g + E_{VI}$) or even the IB as in the case illustrated in figure 4d (the photon energy must exceed just two times E_{VI}, but with E_g still larger than $2E_{VI}$ and thus with E_{VI} larger than E_{IC}).
The variety of possible mechanisms activating MEG in IB solar cells may enhance MEG, which can occur at different E_{th} if the IB is present. Thus, the interplay between IB and MEG in colloidal nanoparticles is promising to further increase the solar cell efficiency.

4 Colloidal nanoparticles for energy harvesting applications

4.1 Core-shell nanoparticles

It has become evident that the surface of the **nanocrystals plays** a crucial role in determining the electronic and optical properties of the nanocomposites. If the surface of the nanocrystals introduces undesired surface states, it needs to be passivated. Moreover, higher reactivity of the surface atoms, particularly when they have dangling bonds, may cause thermodynamic instability of the particles and provoke photodegradation. In the late **'90s,** a possible solution has been proposed [45] and quickly adopted **by** many groups to passivate the surface states of the nanoparticles: a nanometer-thick shell was used to cap the nanoparticles. The approach not only ensures the surface passivation of the nanocrystals, hindering the formation of surface trap but also protects the core of the **nanocrystals** from undesirable chemical activity, e.g., **oxidation** of the surface. Because of the initial aim of the shell, which should protect the core, it was typically made up of a nanometer-thick shell of wider-gap semiconductor, **i.e.** ZnS, as compared to the core semiconductor, i.e. CdSe. This ensured that the shell is a "transparent" layer passivating the core surface and improving electron-hole confinement: both the electron and hole wavefunctions are confined within the core; this is a type I heterojunction, as illustrated in figure 5.
The utility of the core-shell nanoparticles is not limited to the passivation of the nanocrystal surface, but they offer an **additional** degree of tunability, which may result **in precious to improvements** of both MEG and IB absorption. In fact, changing the semiconducting materials composing the core and the shell, typically II-VI or III-V compounds, other types of **heterostructures** can be formed, as illustrated in figure 5. A very promising heterostructure for MEG is the type II heterostructure: in this type, the band alignment between the core and the shell semiconductors results in a spatial separation between the two carriers. Being both the CB and VB edges of the core higher (lower) than those **of** the shell, in this type, the hole (electron) wavefunctions

are confined within the core, while the distribution of electrons (holes) is centered in the shell and decays in the core. If the conduction (valence) band offset is small in type-II heterostructures, electrons (holes) wavefunctions are spread over the entire nanoparticle, while the holes (electrons) wavefunctions are confined in the core (shell): this is referred to as a quasi-type-II heterostructure. A quasi-type II heterostructure was exploited by

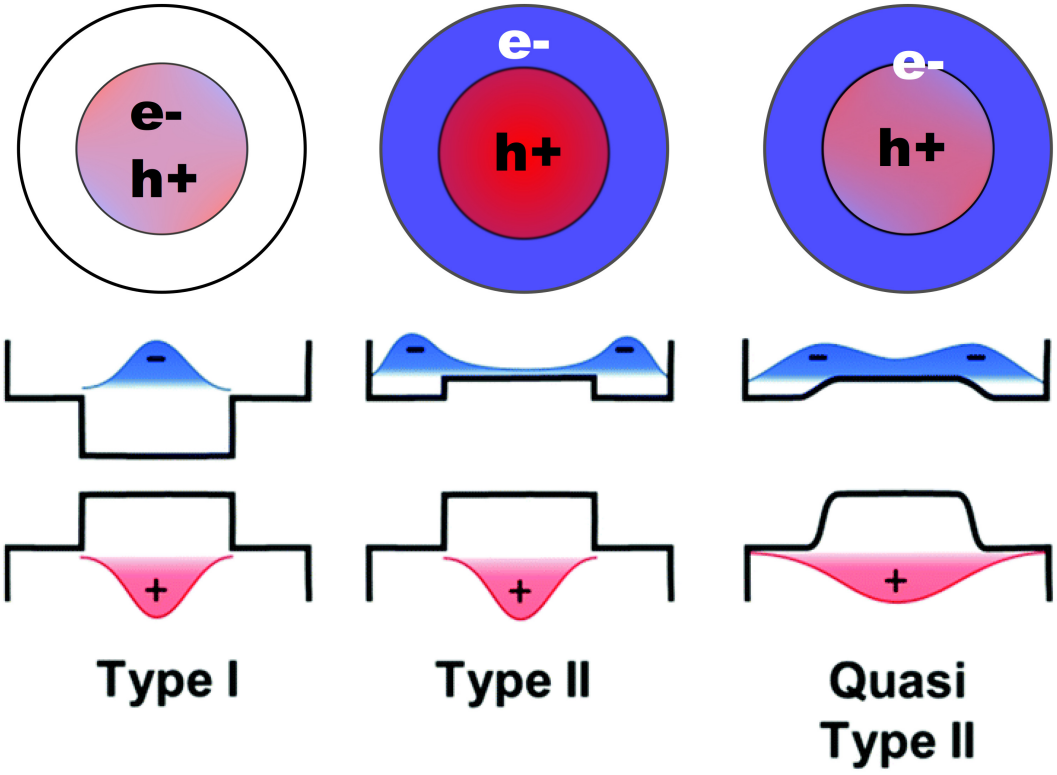

Figure 5. Core/shell nanoparticles forming different types of heterostructures. Schematics of their energy band diagrams with **the** possible electron (blue curves) and hole (red curves) wavefunctions are illustrated. Adapted with permission from [46]. Copyright(2017) Royal Society of Chemistry.

Cirloganu *et al.*[24] to improve MEG rate as compared to a homogeneous **nanoparticle**. These authors proposed PbSe/CdSe core/shell nanoparticles to create the quasi-type II heterostructure, as illustrated in figure 6a. The alignment of the CB of the core and shell causes the spreading of the electrons wavefunctions over the whole structure, while holes are confined within the core, because of the 1.48eV VB offset. This creates the desired spatial separation discussed in the MEG section, reducing electron-hole recombination. They also discuss that the asymmetric distribution of the excess photon energy between the two carriers ($E_h > E_e$, see figure 6a, could reduce E_{th}. **Another** proposed reason for the enhanced CM is that the pre-existing core-localized valence-band electrons interacting in the CM process are spatially separated by a shorter distance as compared to the case of a homogeneous nanoparticle of the same overall size (see figure

6b). By varying the core and shell size, the authors demonstrated that thick-shell PbSe/CdSe nanostructures do increase the CM yield as compared to conventional PbSe quantum dots, accompanied by a reduction of the CM threshold. In general, this study highlights the importance of engineering the nanoparticle heterostructure to improve the CM rate and slow the cooling of hot carriers.

Note that **nanocrystal heterostructures** can be realized also by **so-called** Janus-

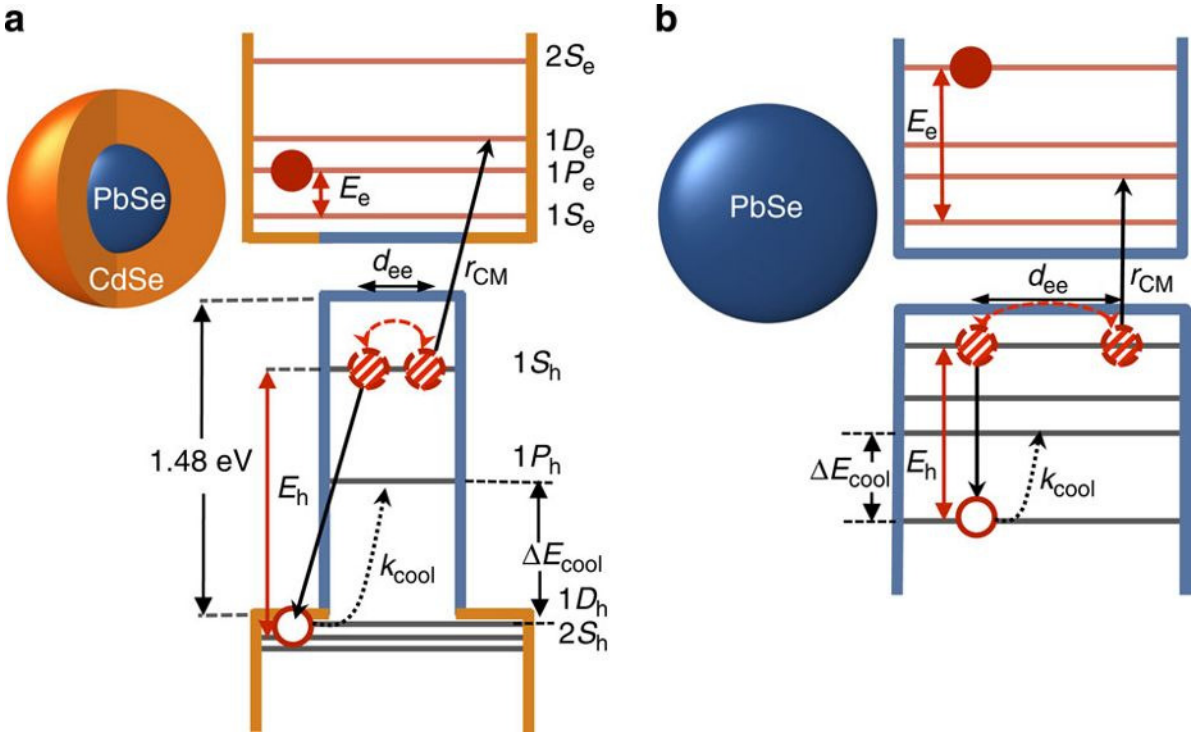

Figure 6. Representation and electronic states of a PbSe/CdSe core/shell nanoparticle **a)** and a homogeneous PbSe nanoparticle **b)** of the same overall size, reproduced from [24]. The photogenerated and pre-existing carriers are shown by solid and dashed circles, respectively.

like nanoparticles, having a spatially asymmetric composition. These nanocrystal heterostructure are not extensively discussed in this review, but we want to stress that heterostructures potentially enabling MEG and IB absorption are not limited to core/shell **nanoparticles** but may involve also asymmetric distributions. Particularly, it was proposed recently that MEG is enhanced in PbS—CdS Janus-like heterostructures as compared to homogeneous and core/shell nanostructures [47].

4.2 All inorganic quantum dot solids

Studying the individual nanoparticles and investigating the different mechanisms (e.g. MEG and IB) that can be exploited by engineering their nanostructure is a crucial step to boost the exploitation of low dimensional structures for solar applications. However, **another** relevant aspect needs to be considered: quantum effects **occur** at

the nanoscale, but the mechanisms activated in the individual nanoparticles needs to be transferred and preserved at the device scale. In other words, excitons have to be turned into carriers, which are then extracted by the contacts to the external circuits. Thus, connecting the nanoparticles and creating a solid layer capable of absorbing photons efficiently, but also transferring and extracting the charge carriers, is **another** paradigm of making solar cells based on colloidal nanoparticles. This is the reason why engineering the nanocrystal ligands [39] has been an important subject in the framework of colloidal nanoparticles. Advances have been made in **recent** years by introducing inorganic ligands, which are very promising for improving charge-carriers mobility in colloidal nanoparticles [48–52]. Particularly, molecular metal chalcogenide complexes, including $Sn_2S_6^{4-}$, $In_2Se_4^{2-}$, AsS_3^{3-} or $Cu_7S_4^{1-}$ [48, 53] have been used to exchange the native long organic ligands on CdSe, CdTe, PbS, InAs or InP nanocrystals, eventually leading to the formation of a semiconducting matrix surrounding the nanocrystals [48, 53–55]. The semiconducting matrix and the nanocrystals form a full-inorganic nanocomposite, which has potentially novel electronic properties. A few additional aspects are important to characterize nanocrystal solids:

(i) a nanocrystal-matrix **heterojunction** is formed, similarly to the case of core-shell nanoparticles, and the whole electronic properties of the nanocomposite are dependent both on the nanocrystal and also much on the embedding matrix (e.g. semiconducting material, crystallinity, stoichiometry) ;

(ii) the role of the nanocrystal-matrix interface, which may introduce electronic states;

(iii) the surface chemistry of the nanoparticle, which may induce the formation of buried interfaces with very different electronic properties as compared to the **surface of the bare nanoparticles**.

Thus, the old view of crystalline semiconducting nanoparticles separated from each **other** but connected by structural intact ligands requires to be replaced by considering a nanocomposite where the dissolution of the ligands create buried interfaces and a new nanocrystalline solid with novel properties.

4.2.1 Group IV nanocrystal/matrix solids

An original theoretical work by Wippermann *et al.*[13] investigated the effect of embedding Si nanoparticles into a semiconducting matrix, i.e. an amorphous, nonstoichiometric ZnS matrix. They reported on the possibility to design nonstoichiometric nanocomposites that exhibit a type II heterojunction at ambient conditions, unlike bulk crystalline Si and ZnS. By means of DFT-molecular dynamics simulations, the author found that after high-temperature annealing (above the melting point of ZnS) of the crystalline ZnS matrix, **segregation** of S atoms at the nanocrystal surface is predicted. Thus, **an** S-capping layer is formed with the missing S atoms in the matrix causing the formation of Zn clusters, which is accompanied by the introduction of electronics states in the matrix band-gap. **Obviously**, these electronic

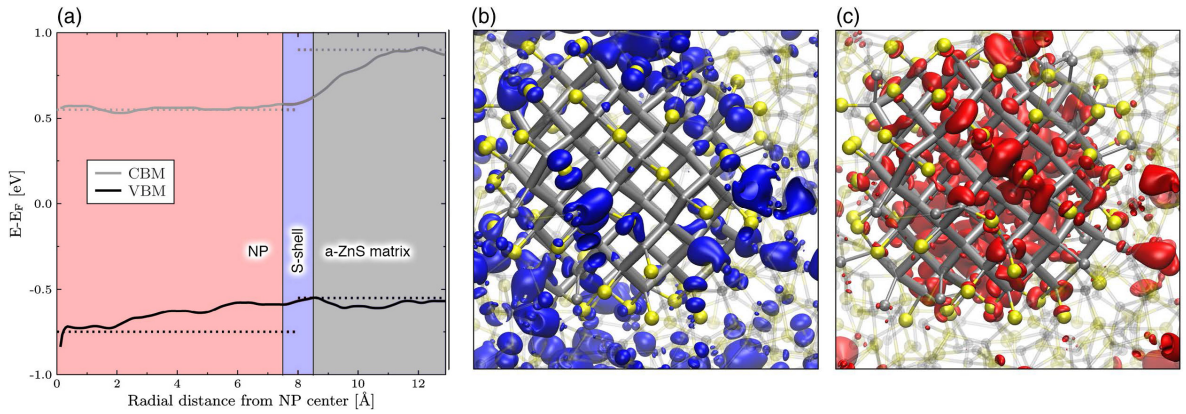

Figure 7. Band alignment between the valence band maximum (VBM) and conduction band minimum (CBM) of the Si nanoparticle and host ZnS matrix (**a**). The isodensity plots of the states at the top of the valence band (blue) and bottom of the conduction band (red) are shown in **b)** and **c)**, respectively, clearly showing the localization of the electron wavefunctions inside the nanocrystals, while the hole wavefunctions are extended over the shell and the ZnS matrix. A ball and stick representation of the Si nanoparticle (**grey** rods) embedded in an a-ZnS matrix has been used, with sulfur atoms (yellow spheres) capping the nanocrystal surface. Reprinted with permission from [13]. Copyright 2014 by the American Physical Society.

states would be very detrimental for photovoltaic devices. The stoichiometry of ZnS matrix was then tuned in order to balance the excess Zn and **re-establish** the local ZnS stoichiometry in the matrix, but with an overall non-stoichiometric ZnS. The non-stoichiometric ZnS matrix embedding the Si nanocrystal was predicted to have **a** well defined electronic gap, without any Zn cluster states, as illustrated in figure 7a. Interestingly, the calculated gap of Si nanocrystals into the ZnS matrix is smaller than the gap of individual Si nanocrystals of the same size or embedded in a silicon oxide matrix, because of the lower quantum-confinement enhancement of the gap caused by the amorphous non-stoichiometric ZnS matrix. Moreover, the band alignment predicted for the nanocomposite shows a type-II heterostructure. In fact, plotting the squared modulus of the wavefunctions, one can clearly see (in figure 7b and 7c that the hole **wavefunctions** are spread over the ZnS matrix and including the S-shell, while the electron wavefunctions are localized inside the core. As already stressed in the previous sections, the spatial separation of the carries would be very beneficial for MEG. But this study gives important general indications for nanocrystal solid systems, other than simply suggesting the Si/ZnS as very promising for solar applications:

(i) embedding the nanocrystals into a semiconducting matrix modifies the electronic properties of the nanocrystal themselves because quantum confinement is affected by the presence of the embedding matrix;

(ii) tuning the composition of the binary semiconducting matrix makes it possible to engineer the heterostructures between the nanocrystals and the hosting matrix

(iii) the surface chemistry plays a crucial role in these systems, e.g. forming shell layers

around the nanoparticle, reducing the sharpness of the heterojunction and strongly modifying the electronic properties of the matrix.

4.2.2 Group III-V nanocrystal/matrix solids

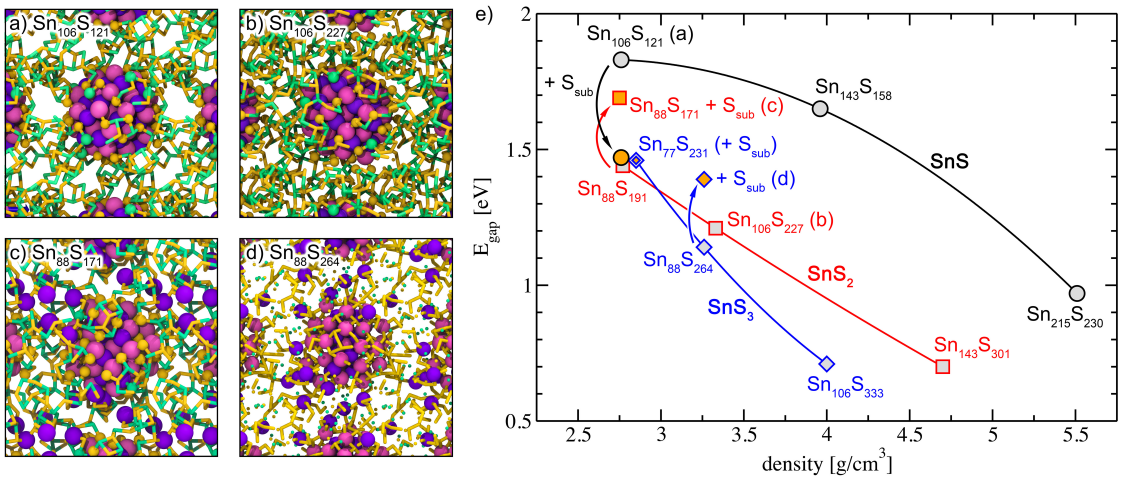

Figure 8. **a)** Schematic representation of a $In_{38}As_{28}$ NC embedded in a dilute amorphous $Sn_{106}S_{121}$ matrix ($\rho_{mat} = 2.8\ g/cm^3$). Magenta and violet spheres, yellow and turquoise rods represent In and As, S and Sn, respectively. **b)** $In_{38}As_{28}$ NC embedded in dilute a-SnS_2 at $\rho_{mat} = 3.3\ g/cm^3$. For SnS_2 and higher S contents, we observe the formation of sulfur chain structures connecting the nanocrystals, possibly explaining the large mobilities observed in recent experiments [48]. **c)** Lower total energies and larger electronic gaps are obtained by introducing subsurface sulfur and corresponding incorporation of As in the matrix during the MD runs (SnS_2 matrix at $\rho_{mat} = 2.8\ g/cm^3$, (sub-)surface S atoms drawn as yellow spheres). **d)** $In_{38}As_{28}$ embedded in a-SnS_3 at $\rho_{mat} = 3.3\ g/cm^3$, showing both sulfur chains and subsurface sulfur. **e)** Dependence of the NC-composite electronic gap on the matrix density, stoichiometry and matrix atomistic structure. Reproduced from [12].

The role of surface chemistry is even more evident in the case of III-V (or II-V) nanocrystals embedded in a semiconducting matrix. Particularly, we studied an archetype system of InAs nanocrystals capped by Sn_2S_6 ligands by a joint experimental and theoretical approach [12]. Firstly, by investigating the thermodynamic stability of the ligands on the nanocrystal surface and the energy diagrams for an interface between the InAs surface and the ligands, we predicted that intact Sn_2S_6 ligands on the nanocrystal surface are not stable and are not absorbed as intact units on the nanocrystal surface. Moreover, DFT-molecular dynamics simulations supported by XPS and Raman experiments evidenced that the Sn_2S_6 ligands decompose and form an amorphous matrix surrounding the InAs nanocrystals (see figure 8a-8d), with S-**segregation** on the nanocrystals, similarly to the case of Si/ZnS nanocomposites, but also with the **adsorption** of S atoms underneath the nanocrystal surface. We found that both the atomistic details and the electronic properties of the nanocomposite can be

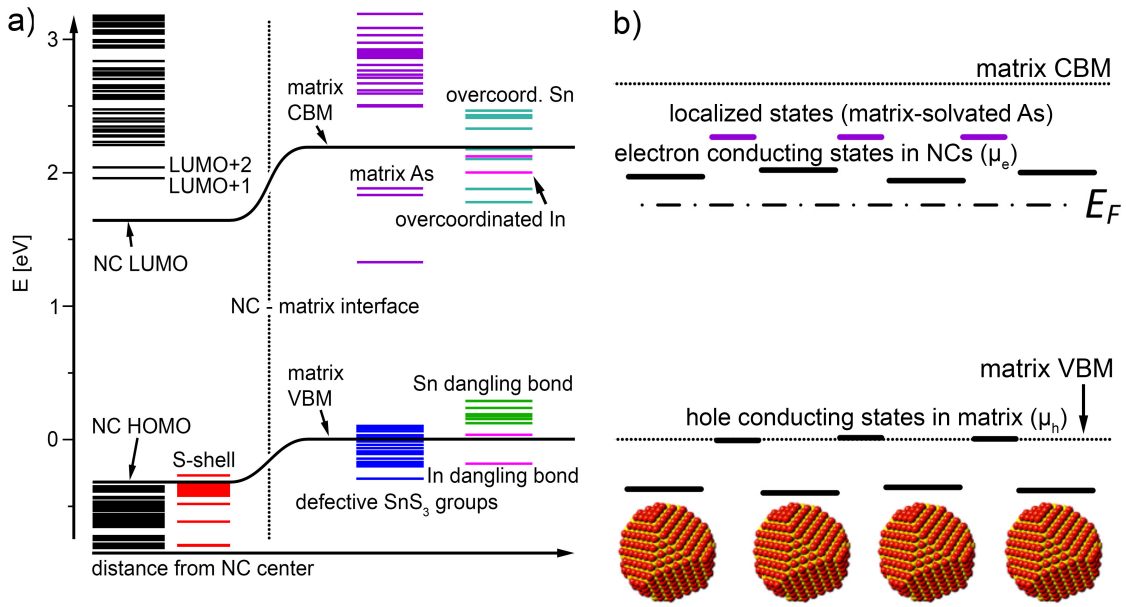

Figure 9. **a)**Energy level alignment at nano-heterojunction between $In_{38}As_{28}$ and $Sn_{88}S_{171}$ matrix. The model contains subsurface S incorporated into the NP and in turn As solvated inside the matrix. In terms of defect states, of particular interest are the levels arising from As occupying a Sn lattice site, in a configuration which otherwise would fulfil electron counting. Compared to Sn, the additional As electron may be accommodated in, e. g., a Sn dangling bond or SnS_3 defect state, with an empty defect state localized to a SnS_3-AsS_3 unit. Note these defects are located above the NC LUMO, which is associated with the mobility edge for majority carriers (electrons), while the hole-conducting states are given by the matrix band edge, as shown in the schematic in **b)**. Reproduced from [12].

tuned by changing the synthesis conditions. In fact, the bandgap of the nanocomposite was predicted to depends on the matrix density and stoichiometry, as illustrated in figure 8e. Notably, the optical **absorption** spectra of inorganic ligand-capped nanocrystals in solution changes when the nanocrystals are embedded in the solid and a number of defect states were identified in the latter case, as illustrated in figure 9a. Some of these defects states highlight the impact of the nanoparticle surface chemistry on the electronic and optical properties of the nanocomposite: we found that localized donor states above the mobility edge, which were proposed as one of the factors causing the negative photoconductive probed experimentally [12, 48], are provided by matrix-solvated As (see figure 9a and 9b). Arsenic preferentially occupies a Sn lattice site, leading to corner-sharing SnS_3 and AsS_3 groups, in a configuration that without As substitution would satisfy electron counting. Compared to Sn, we propose that the additional As electron is accommodated in an acceptor state given by, e. g., a Sn dangling bond or SnS_3 defect state. The empty matrix-As states with **the** lowest energy are often located energetically between the nanocrystal LUMO and LUMO+1/+2 states but below the matrix CBM. Ultimately, the origin of these trap states can be **inreferred** to **the** subsurface sulfur formation, which in turn gives rise to matrix-solvated As. We

also predicted that increasing the matrix stoichiometry towards SnS_3 the formation of S-chains is promoted, as shown in figure 8d, which improve the hole transport due to the formation of hole-conducting interconnects through the matrix.
Finally, it is important to note that the predicted band alignment at the nanoparticle-matrix shows a type II heterojunction, (see figure 9a), leading to charge-separated transport channels for electrons and holes. In the schematic of figure 9b) it is evident that in the nanocrystal solid the mobility edge for electrons is associated with the nanocrystal LUMO states, enabling hopping transport from NC to NC for electrons, while the hole conducting states are given by the matrix band edge leading to band-like transport for holes.

5 Conclusions

Both MEG and IB absorption **has** been demonstrated as promising mechanisms capable of increasing the rate of photogenerated carriers in solar cells. It is still not evident the impact of these phenomena on the final performance of the devices, and it is not clear if relevant improvements can be reached. Thus, both experiments and theoretical models are necessary to probe the real impact that MEG and IB absorption can have on the real and final solar devices, particularly for the case in which both effects (MEG and IB) are exploited at the same time. Combining both up- and down-conversion is indeed a promising approach to maximize their impact on photovoltaics, which needs further investigations.
Nanocrystal solids composed by semiconducting group IV, III-V and II-VI are very interesting systems for optoelectronic applications and photovoltaics. Particularly, because of the high tunability of their electronic properties together and the intrinsic quantum nature of the nanocrystals, they are an excellent platform for studying fundamental exciton phenomena and implementing third-generation photovoltaic cells based on MEG and IB absorption. This was demonstrated by the two cases of study discussed above.
These studies **show** how the formation of a full inorganic nanocrystal solid cannot be thought as a simple sum of the nanocrystals and intact inorganic ligands. The organic-inorganic ligand exchange process and the solid film synthesis are crucial for the properties of the final nanocomposite, because of the fundamental role of the nanocrystal surface chemistry. Different complex **mechanisms** are involved in the surface chemistry of the nanocrystal solid, including segregation processes between matrix and nanocrystals, the absorption of atoms at the nanocrystal (sub)surface, the formation of **sub-stoichiometric** region or conductive cluster/chains in the matrix. All these **mechanisms** need to be studied for any specific system under investigation and details at the atomistic levels are fundamental for understanding experimental **behaviours**.

6 References

[1] Talapin D V and Murray C B 2005 *Science* **310** 86–89 ISSN 0036-8075 (*Preprint* http://science.sciencemag.org/content/310/5745/86.full.pdf) URL http://science.sciencemag.org/content/310/5745/86

[2] Sargent E H 2012 *Nature Photonics* **6** 133–135 ISSN 1749-4885 URL http://www.nature.com/articles/nphoton.2012.33

[3] Michalet X, Pinaud F F, Bentolila L A, Tsay J M, Doose S, Li J J, Iyer G and Weiss S 2005 Peptide-coated semiconductor nanocrystals for biomedical applications vol 5704 ed Bornhop D J, Achilefu S I, Raghavachari R and Savitsky A P (International Society for Optics and Photonics) p 57 URL http://proceedings.spiedigitallibrary.org/proceeding.aspx?doi=10.1117/12.589498

[4] McDonald S A, Konstantatos G, Zhang S, Cyr P W, Klem E J D, Levina L and Sargent E H 2005 *Nature Materials* **4** 138–142 ISSN 1476-1122 URL http://www.nature.com/articles/nmat1299

[5] Park J, Joo J, Kwon S, Jang Y and Hyeon T 2007 *Angewandte Chemie International Edition* **46** 4630–4660 ISSN 1521-3773 URL http://dx.doi.org/10.1002/anie.200603148

[6] Yin Y and Alivisatos A P 2005 *Nature* **437** 664–670 URL http://dx.doi.org/10.1038/nature04165

[7] Murray C B, Kagan C R and Bawendi M G 2000 *Annual Review of Materials Science* **30** 545–610 (*Preprint* http://dx.doi.org/10.1146/annurev.matsci.30.1.545) URL http://dx.doi.org/10.1146/annurev.matsci.30.1.545

[8] Srivastava V, Janke E M, Diroll B T, Schaller R D and Talapin D V 2016 *Chemistry of Materials* **28** 6797–6802 ISSN 0897-4756 URL http://pubs.acs.org/doi/10.1021/acs.chemmater.6b03501

[9] Taleb Mokari , , Minjuan Zhang and Peidong Yang* 2007 URL https://pubs.acs.org/doi/10.1021/ja074145i

[10] Yu W W, Wang Y A and Peng X 2003 URL https://pubs.acs.org/sharingguidelines

[11] Boles M A and Talapin D V 2014 *Science* **344** 1340–1341 ISSN 0036-8075 (*Preprint* http://science.sciencemag.org/content/344/6190/1340.full.pdf) URL http://science.sciencemag.org/content/344/6190/1340

[12] Scalise E, Srivastava V, Janke E, Talapin D, Galli G and Wippermann S *Nature Nanotechnology* URL https://www.nature.com/articles/s41565-018-0189-9.pdf

[13] Wippermann S, Vörös M, Gali A, Gygi F, Zimanyi G T and Galli G 2014 *Phys. Rev. Lett.* **112**(10) 106801 URL https://link.aps.org/doi/10.1103/PhysRevLett.112.106801

[14] Alharbi F H and Kais S 2015 *Renewable and Sustainable Energy Reviews* **43** 1073 – 1089 ISSN 1364-0321 URL http://www.sciencedirect.com/science/article/pii/S136403211401048X

[15] Shockley W and Queisser H J 1961 *Journal of Applied Physics* **32** 510–519 (*Preprint* https://doi.org/10.1063/1.1736034) URL https://doi.org/10.1063/1.1736034

[16] Yoshikawa K, Kawasaki H, Yoshida W, Irie T, Konishi K, Nakano K, Uto T, Adachi D, Kanematsu M, Uzu H and Yamamoto K 2017 *Nature Energy* **2** 17032 ISSN 2058-7546 URL http://www.nature.com/articles/nenergy201732

[17] Siemons N and Serafini A 2018 *Journal of Nanotechnology* **2018** 1–12 ISSN 1687-9503 URL https://www.hindawi.com/journals/jnt/2018/7285483/

[18] Goodwin H, Jellicoe T C, Davis N J and Böhm M L 2018 *Nanophotonics* **7** 111–126 ISSN 2192-8614 URL http://www.degruyter.com/view/j/nanoph.2018.7.issue-1/nanoph-2017-0034/nanoph-2017-0034.xml

[19] Wolff P A 1954 *Physical Review* **95** 1415–1420

[20] Doany F E and Grischkowsky D 1988 *Applied Physics Letters* **52** 36–38 (*Preprint* https://doi.org/10.1063/1.99309) URL https://doi.org/10.1063/1.99309

[21] Beard M C, Midgett A G, Hanna M C, Luther J M, Hughes B K and Nozik A J 2010 *Nano Letters* **10** 3019–3027 pMID: 20698615 (*Preprint* https://doi.org/10.1021/nl101490z) URL https://doi.org/10.1021/nl101490z

[22] Nozik A 2002 *Physica E: Low-dimensional Systems and Nanostructures* **14** 115 – 120 ISSN 1386-9477 URL http://www.sciencedirect.com/science/article/pii/S1386947702003740

[23] Kumar M, Vezzoli S, Wang Z, Chaudhary V, Ramanujan R V, Gurzadyan G G, Bruno A and Soci C 2016 *Physical Chemistry Chemical Physics* **18** 31107–31114 ISSN 1463-9076 URL http://xlink.rsc.org/?DOI=C6CP03790A

[24] Cirloganu C M, Padilha L A, Lin Q, Makarov N S, Velizhanin K A, Luo H, Robel I, Pietryga J M and Klimov V I 2014 *Nature Communications* **5** 4148 ISSN 2041-1723 URL http://www.nature.com/articles/ncomms5148

[25] Richard D Schaller, Milan Sykora, , Jeffrey M Pietryga and Klimov* V I 2006 URL https://pubs.acs.org/doi/abs/10.1021/nl052276g

[26] Randy J Ellingson * , Matthew C Beard * , Justin C Johnson , Pingrong Yu , Olga I Micic , Arthur J Nozik * , , Andrew Shabaev § and Alexander L Efros* § 2005 URL https://pubs.acs.org/doi/abs/10.1021/nl0502672

[27] Schaller R D and Klimov V I 2004 *Physical Review Letters* **92** 186601 ISSN 0031-9007 URL https://link.aps.org/doi/10.1103/PhysRevLett.92.186601

[28] Nozik A J 2001 SPECTROSCOPY AND HOT ELECTRON RELAXATION DYNAMICS IN SEMICONDUCTOR QUANTUM WELLS AND QUANTUM DOTS Tech. rep. URL www.annualreviews.org

[29] Rogach A L 2008 *Semiconductor Nanocrystal Quantum Dots* ISBN 9783211752357 URL http://link.springer.com/10.1007/978-3-211-75237-1%5Cnhttp://www.springerlink.com/index/10.1007/97

[30] Efros A L, Kharchenko V A and Rosen M 1995 *Solid State Communications* **93** 281–284 ISSN 00381098

[31] Klimov V I 2002 *The Journal of Physical Chemistry B* **104** 6112–6123 ISSN 1520-6106

[32] Kumar M, Vezzoli S, Wang Z, Chaudhary V, Ramanujan R V, Gurzadyan G G, Bruno A and Soci C 2016 *Phys. Chem. Chem. Phys* **18** 31107 URL www.rsc.org/pccp

[33] Geiregat P, Delerue C, Justo Y, Aerts M, Spoor F, Dries, Thourhout V, Siebbeles L D A, Allan G, Houtepen A J and Hens Z 2015 URL www.acsnano.org778

[34] Luque A and Martí A 1997 Increasing the Efficiency of Ideal Solar Cells by Photon Induced Transitions at Intermediate Levels Tech. rep. URL https://journals.aps.org/prl/pdf/10.1103/PhysRevLett.78.5014

[35] Okada Y, Ekins-Daukes N J, Kita T, Tamaki R, Yoshida M, Pusch A, Hess O, Phillips C C, Farrell D J, Yoshida K, Ahsan N, Shoji Y, Sogabe T and Guillemoles J F 2015 *Applied Physics Reviews* **2** ISSN 19319401

[36] Martí A, Antolín E, Stanley C R, Farmer C D, López N, Díaz P, Cánovas E, Linares P G and Luque A 2006 URL https://journals.aps.org/prl/pdf/10.1103/PhysRevLett.97.247701

[37] Vörös M, Galli G and Zimanyi G T 2015 *ACS Nano* **9** 6882–6890 ISSN 1936-0851 URL http://pubs.acs.org/doi/10.1021/acsnano.5b00332

[38] Talapin D V, Lee J S, Kovalenko M V and Shevchenko E V 2010 *Chemical Reviews* ISSN 00092665

[39] Wang R, Shang Y, Kanjanaboos P, Zhou W, Ning Z and Sargent E H 2016 *Energy & Environmental Science* **9** 1130–1143 ISSN 1754-5692 URL http://xlink.rsc.org/?DOI=C5EE03887A

[40] Liu Y, Gibbs M, Puthussery J, Gaik S, Ihly R, Hillhouse H W and Law M 2010 *Nano Letters* **10** 1960–1969 ISSN 1530-6984 URL https://pubs.acs.org/doi/10.1021/nl101284k

[41] Santra P K and Kamat P V 2012 *Journal of the American Chemical Society* **134** 2508–2511 ISSN 0002-7863 URL http://pubs.acs.org/doi/10.1021/ja211224s

[42] Vörös M, Rocca D, Galli G, Zimanyi G T and Gali A 2013 *Physical Review B* **87** 155402 ISSN 1098-0121 URL https://link.aps.org/doi/10.1103/PhysRevB.87.155402

[43] Sullivan J T, Simmons C B, Buonassisi T and Krich J J 2015 *IEEE Journal of Photovoltaics* ISSN 21563381

[44] Engel J H and Alivisatos A P 2014 Postsynthetic doping control of nanocrystal thin films: Balancing space charge to improve photovoltaic efficiency

[45] Hines M A and Guyot-Sionnest P 1996 *The Journal of Physical Chemistry* **100** 468–471 ISSN

0022-3654 URL https://pubs.acs.org/doi/10.1021/jp9530562

[46] Jang Y, Shapiro A, Isarov M, Rubin-Brusilovski A, Safran A, Budniak A K, Horani F, Dehnel J, Sashchiuk A and Lifshitz E 2017 *Chem. Commun* **53** 1002 URL www.rsc.org/chemcomm

[47] Kroupa D M, Pach G F, Vörös M, Giberti F, Chernomordik B D, Crisp R W, Nozik A J, Johnson J C, Singh R, Klimov V I, Galli G and Beard M C 2018 *ACS Nano* **12** 10084–10094 ISSN 1936-0851 URL http://pubs.acs.org/doi/10.1021/acsnano.8b04850

[48] Liu W, Lee J S and Talapin D V 2013 *Journal of the American Chemical Society* **135** 1349–1357 pMID: 23267673 (*Preprint* http://dx.doi.org/10.1021/ja308200f) URL http://dx.doi.org/10.1021/ja308200f

[49] Lee J S, Kovalenko M V, Huang J, Chung D S and Talapin D V 2011 *Nat Nano* **6** 348–352 URL http://dx.doi.org/10.1038/nnano.2011.46

[50] Chung D S, Lee J S, Huang J, Nag A, Ithurria S and Talapin D V 2012 *Nano Letters* **12** 1813–1820 pMID: 22385132 (*Preprint* http://dx.doi.org/10.1021/nl203949n) URL http://dx.doi.org/10.1021/nl203949n

[51] Huang J, Liu W, Dolzhnikov D S, Protesescu L, Kovalenko M V, Koo B, Chattopadhyay S, Shenchenko E V and Talapin D V 2014 *ACS Nano* **8** 9388–9402 pMID: 25181260 (*Preprint* http://dx.doi.org/10.1021/nn503458y) URL http://dx.doi.org/10.1021/nn503458y

[52] Cordones A A, Scheele M, Alivisatos A P and Leone S R 2012 *Journal of the American Chemical Society* **134** 18366–18373 pMID: 23072613 (*Preprint* http://dx.doi.org/10.1021/ja3071732) URL http://dx.doi.org/10.1021/ja3071732

[53] Kovalenko M V, Bodnarchuk M I, Zaumseil J, Lee J S and Talapin D V 2010 *Journal of the American Chemical Society* **132** 10085

[54] Lee J S, Kovalenko M V, Huang J, Chung D S and Talapin D V 2011 *Nat Nano* **6** 348–352 URL http://dx.doi.org/10.1038/nnano.2011.46

[55] Ip A H, Thon S M, Hoogland S, Voznyy O, Zhitomirsky D, Debnath R, Levina L, Rollny L R, Carey G H, Fischer A, Kemp K W, Kramer I J, Ning Z, Labelle A J, Chou K W, Amassian A and Sargent E H 2012 *Nat Nano* **7** 577–582 URL http://dx.doi.org/10.1038/nnano.2012.127